

Radical or Not Radical: Compared Structures of Metal (M = Ni, Au) Bis-Dithiolene Complexes with a Thiazole Backbone

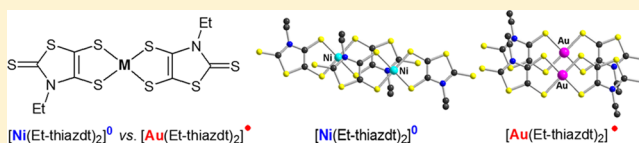
Agathe Filatre-Furcate,[†] Nathalie Bellec,[†] Olivier Jeannin,[†] Pascale Auban-Senzier,[‡] Marc Fourmigué,[†] Antoine Vacher,[†] and Dominique Lorcy^{*,†}

[†]Institut des Sciences Chimiques de Rennes, UMR 6226 CNRS-Université de Rennes 1, Campus de Beaulieu, Bât 10A, 35042 Rennes Cedex, France

[‡]Laboratoire de Physique des Solides UMR 8502 CNRS-Université de Paris-Sud, Bat 510, F-91405 Orsay Cedex, France

S Supporting Information

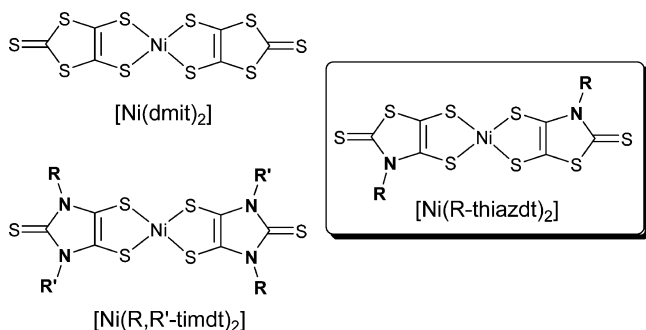
ABSTRACT: A complete series of dianionic, monoanionic, and neutral dithiolene complexes formulated as $[\text{Ni}(\text{Et-thiazdt})_2]^n$, with $n = -2, -1, 0$, and Et-thiazdt: *N*-ethyl-1,3-thiazoline-2-thione-4,5-dithiolate, is prepared using an optimized procedure described earlier for the *N*-Me derivatives. Electrochemical and spectroscopic properties confirm the electron-rich character of the Et-thiazdt dithiolate ligand. The three complexes are structurally characterized by single-crystal X-ray diffraction. The paramagnetic anionic complex $[\text{Ni}(\text{Et-thiazdt})_2]^{-1}$, as Ph_4P^+ salt, exhibits side-by-side lateral interactions leading to a Heisenberg spin chain behavior. The solid-state structure of the neutral, diamagnetic $[\text{Ni}(\text{Et-thiazdt})_2]^0$ complex shows a face-to-face organization with a large longitudinal shift, at variance with the structure of its radical and neutral gold dithiolene analogue described earlier and formulated as $[\text{Au}(\text{Et-thiazdt})_2]^0$. Comparison of the two structures, and those of the other few structurally characterized pairs of Ni/Au dithiolene complexes, demonstrates the important role played by overlap interactions between gold dithiolene radical species. Despite its closed-shell character, the neutral nickel complex $[\text{Ni}(\text{Et-thiazdt})_2]^0$ exhibits a semiconducting behavior with a room-temperature conductivity $\sigma_{\text{RT}} \approx 0.014 \text{ S cm}^{-1}$.



INTRODUCTION

Nickel bis(dithiolene) complexes have been intensively studied as precursors of molecular conductors, and one prototypical complex within this class of molecules is $\text{Ni}(\text{dmit})_2$.^{1–3} Various modifications of the dithiolene skeleton have been performed in order to modulate the redox properties of the complex and therefore also the electronic properties of the materials.^{4,5} An interesting, but poorly explored so far, class of metal bis(dithiolene) complexes is based on the electron-rich ligand *N*-alkyl-1,3-thiazoline-2-thione-4,5-dithiolate (*R*-thiazdt), noted hereafter as $[\text{M}(\text{R-thiazdt})_2]$ (Chart 1). It combines an electron-rich character favoring the isolation of highly oxidized species, together with a structural flexibility brought by the

Chart 1



substituent on the nitrogen atom, an attractive situation intermediate between anionic or neutral $[\text{Ni}(\text{dmit})_2]^n$ ($n = -2, -1, -0.5, 0$) complexes and the neutral or cationic $[\text{Ni}(\text{timdt})_2]^n$ ($n = 0, +1$), where timdt is the monoanion of *R,R'* disubstituted imidazolidine-2,4,5-trithione.⁶

The $[\text{Ni}(\text{R-thiazdt})_2]$ complex was first reported by Arca et al. with $\text{R} = \text{Et}$. Its preparation involved the sulfuration of the *N*-ethyl-2-thioxothiazolidine-4,5-dione with Lawesson's reagent in the presence of nickel or nickel salts, affording the corresponding $[\text{Ni}(\text{Et-thiazdt})_2]$ as the neutral species in rather low yield (15%).⁷ This $\text{R} = \text{Et}$ complex was not structurally characterized, neither in its neutral form, nor in its mono- or dianionic forms. More recently, we also investigated the synthesis of the same class of Ni complexes with a methyl group on the ligand ($\text{R} = \text{Me}$),⁸ with a different synthetic approach. Indeed, the dianionic dithiolate ligand was first prepared and reacted with a Ni^{2+} salt to generate directly the most reduced form as the dianionic species, i.e. $[\text{Ni}(\text{Me-thiazdt})_2]^{2-}$. This approach allowed us to structurally characterize the dianionic species, and following one-electron oxidation, the radical anion species $[\text{Ni}(\text{Me-thiazdt})_2]^{-\bullet}$. Besides, we also investigated the synthesis of analogous gold dithiolene complexes, as monoanionic and neutral complexes, $[\text{Au}(\text{Et-thiazdt})_2]^{-1,0}$. The neutral radical species proved to be particularly interesting as it exhibits a peculiar two-dimensional

Received: June 3, 2014

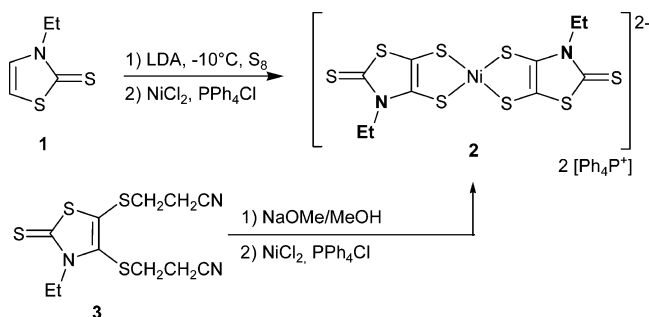
Published: July 30, 2014

solid-state organization, associated with a very high conductivity, and a transition to a metallic state under pressure.⁹ Chalcogen substitution in the thiazole ring also allowed for the construction of a rich phase diagram with these series of single-component neutral radical species $[\text{Au}(\text{Et-thiazdt})_2]^\bullet$.¹⁰ At this stage, it was becoming interesting to also have at hand the analogous nickel complexes with $R = \text{Et}$, and particularly their structural properties, in order to evaluate the role of the metal (Ni vs Au) in their solid-state associations, particularly between the diamagnetic $[\text{Ni}(\text{Et-thiazdt})_2]^0$ and the paramagnetic $[\text{Au}(\text{Et-thiazdt})_2]^\bullet$ complexes. On these bases, we reinvestigated the preparation of the nickel complex with $R = \text{Et}$ in the hope to characterize the complete series from the dianion to the neutral complex.

RESULTS AND DISCUSSION

Syntheses. The approach to the target molecule was based on our previous synthesis of the $[\text{Ni}(\text{Me-thiazdt})_2]^{2-}$,⁸ and involves the *N*-ethyl-1,3-thiazoline-2-thione 1,⁹ as outlined in Scheme 1. The dithiolate was formed by treating *N*-ethyl-1,3-

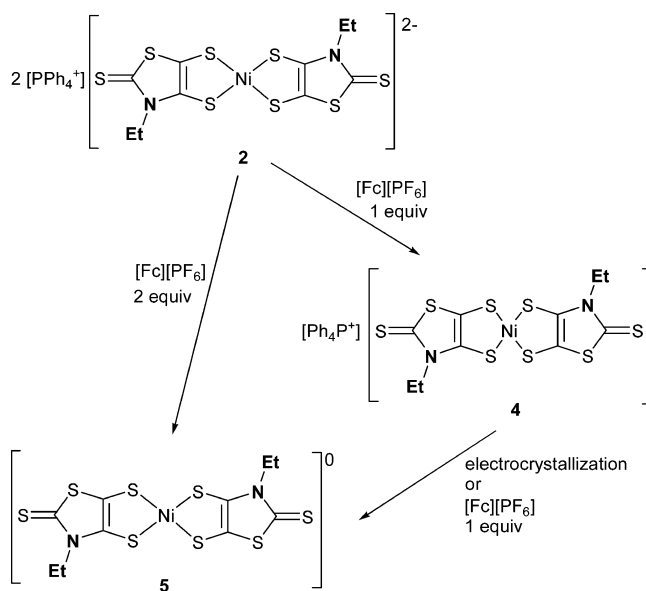
Scheme 1. Preparation of the Dianionic Complex 2 as PPh_4^+ Salt



thiazoline-2-thione 1 at -10°C in THF in a two-step procedure, by adding successively 1.5 equiv of lithium diisopropylamide (LDA) and sulfur, twice (Scheme 1). Then NiCl_2 was added to the solution, followed by the addition of PPh_4Cl to afford the corresponding salt of the dianionic species, $[\text{PPh}_4]_2[\text{Ni}(\text{Et-thiazdt})_2]$ 2 in 17% yield as dark red powder. Another approach starting from the *N*-ethyl-bis-(cyanoethylthio)-1,3-thiazoline-2-thione 3,⁹ with the two thiolate functions protected by cyanoethyl groups, proved more interesting. Deprotection of the thiolate functions in the presence of sodium methanolate, followed by the addition of NiCl_2 and PPh_4Cl allowed us to isolate the dithiolene complexes 2 in 52% yield (Scheme 1). This complex 2 was recrystallized in acetonitrile. As already observed for the *N*-Me analogue of this complex, $[\text{NEt}_4]_2[\text{Ni}(\text{Me-thiazdt})_2]$, the dianionic complex 2 is easily oxidized in solution upon air exposure into the anion radical species (vide infra).

The monoanionic salt 4 was generated by adding 1 equiv of $[\text{Cp}_2\text{Fe}][\text{PF}_6]$ to a dichloromethane solution of 2 (Scheme 2). Following this procedure, we isolated the monoanionic complex 4, $[\text{PPh}_4][\text{Ni}(\text{Et-thiazdt})_2]$, in 71% yield as dark red powder. Two different approaches were developed for the neutral species $[\text{Ni}(\text{Et-thiazdt})_2]^0$ (5) (Scheme 2), (i) the direct chemical oxidation of the dianionic complex 2 with two equivalents $[\text{Cp}_2\text{Fe}][\text{PF}_6]$ and recrystallization to give $[\text{Ni}(\text{Et-thiazdt})_2]$ (5), and (ii) the sequential oxidation to the monoanionic complex 4 with one equivalent $[\text{Cp}_2\text{Fe}][\text{PF}_6]$,

Scheme 2. Preparation of the Monoanionic 4 and Neutral 5 Ni Complexes



followed by electrocrystallization of this intermediate complex 4 to the neutral species 5 $[\text{Ni}(\text{Et-thiazdt})_2]$, isolated as tiny black crystals at the anode.

Electrochemical Properties. The redox properties of the Ni complexes were investigated, either starting from the dianionic species 2 or from the monoanionic one 4, by cyclic voltammetry experiments performed in CH_2Cl_2 using $[\text{NBu}_4][\text{PF}_6]$ as supporting electrolyte with potentials given in V vs. SCE. On the cyclic voltammogram reported in Figure 1, three

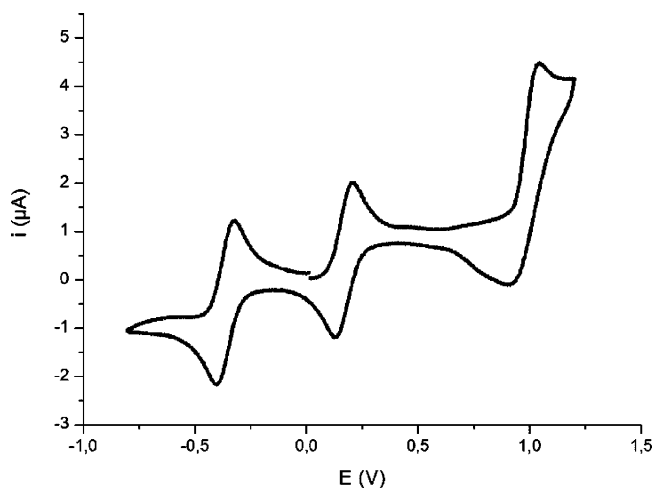


Figure 1. Cyclic voltammogram of $[\text{PPh}_4][\text{Ni}(\text{Et-thiazdt})_2]$ in CH_2Cl_2 with $[\text{NBu}_4][\text{PF}_6]$ 0.1 M as electrolyte, E in V vs SCE. Scan rate = 100 mV s^{-1} .

redox processes can be observed, the two first one being fully reversible monoelectronic transfers and the third most anodic one is not fully reversible. The two first processes are ascribed to the oxidation of successively the dianion into the monoanion radical at $E_1(-2/-1) = -0.37\text{ V}$ versus SCE and of the monoanion into the neutral species at $E_2(-1/0) = 0.175\text{ V}$ versus SCE. These two redox waves were already reported by Arca et al. ($E_1(-2/-1) = -0.814(3)$; $E_2(-1/0) \cong -0.280(2)\text{ V}$

vs Fc/Fc^+). The third process, not mentioned earlier, is associated with the oxidation of the neutral species into the cation radical one. This is actually possible because of the presence of the two electron rich dithiolene ligands, Et-thiazdt. Indeed, as observed for other Ni bis(dithiolene) complexes with electron-rich dithiolate ligands (Table 1), the cathodic

Table 1. Redox Potentials for the Ni Complexes in CH_2Cl_2 with $[\text{NBu}_4][\text{PF}_6]$ 0.1 M, E in V vs SCE with Scan Rate = 100 mV s^{-1}

	E^1	E^2	E_{pa}^3	ref
$[\text{Ni}(\text{dmit})_2]^b$	-0.175	+0.34/0.228 ^c		11
$[\text{Ni}(\text{Et-thiazdt})_2]$	-0.37	+0.175	+1.12 ^a	this work
$[\text{Ni}(\text{Me-thiazdt})_2]$	-0.34	0.22/0.00 ^c		8
$[\text{Ni}(\text{Et}_2\text{-timdt})_2]$	-0.56	-0.11	+0.78	12
$[\text{Ni}(\text{DL-bordt})_2]^d$	-1.20	-0.43	+1.00 ^a	13

^aNot a fully reversible process. ^b E values have been determined in CH_3CN . ^c $E_{\text{pa}}/E_{\text{pc}}$: anodic and cathodic peak potentials. ^dDL-bordt stands for bornylenedithiolate.

shift observed for the two first oxidation processes ($-2/-1$) and ($-1/0$) allows for the observation of the ($0/+1$) oxidation process within the potential window. As expected, comparison of the redox potentials of the $[\text{Ni}(\text{Et-thiazdt})_2]$ complex with those of the methyl analogue, $[\text{Ni}(\text{Me-thiazdt})_2]$ investigated in the same conditions, shows no significant differences. Nevertheless, it should be noted that for the $[\text{Ni}(\text{Me-thiazdt})_2]$ the oxidation of the radical anion to the neutral species was not fully reversible as a result of the adsorption phenomenon.

UV-vis-NIR Spectroelectrochemical Properties. The absorption properties of the three species (e.g., dianionic, anion radical, and neutral) were first measured in CH_2Cl_2 at room temperature. For the dianionic complex, freshly prepared solutions of **2** exhibit absorption bands in the UV-vis region only. Contrariwise, the monoanionic complex **4** and the neutral complex **5** exhibit a strong electronic absorption in the NIR region at 1280 nm ($\epsilon = 2.1 \times 10^4 \text{ M}^{-1} \text{ cm}^{-1}$) and 1022 nm ($\epsilon = 5.5 \times 10^4 \text{ M}^{-1} \text{ cm}^{-1}$), respectively. UV-vis-NIR spectroelectrochemical investigations were carried out on the dianionic complex in CH_2Cl_2 - $[\text{NBu}_4][\text{PF}_6]$ 0.2 M solution (Figure 2). It is worth noting that because of its redox potential, this dianionic complex **2** is easily oxidized in solution to the anion radical species **4** in the presence of air. This explains why, under an applied potential of -0.4 V , the NIR absorption band of the monoanionic species can be already observed. The gradual oxidation of the dianionic complex **2** to the radical anion induces the growth of this low energy band characteristic of the monoanionic complex **4** in the NIR at 1280 nm. This intense band is assigned to ligand-localized $\pi-\pi^*$ transitions. Upon oxidation to the neutral species, the band localized at 1280 nm gradually decreases, whereas a novel band at higher energy emerges on the spectra at 1022 nm. Attempts to oxidize the neutral complex **5** to the monocationic species induces a decrease of all the absorption bands in accordance with a degradation of the generated product, as already observed on the CV by the irreversible character of this ($0/+1$) process.

Structural Properties. Crystals have been obtained for all three complexes. The dianionic salt **2**, $[\text{PPh}_4]_2[\text{Ni}(\text{Et-thiazdt})_2]$, was recrystallized from acetonitrile, although single crystals of the radical anion salt **4**, $[\text{PPh}_4][\text{Ni}(\text{Et-thiazdt})_2]$ and the neutral complex **5**, $[\text{Ni}(\text{Me-thiazdt})_2]$ were obtained by recrystallization into a toluene/acetonitrile solution (1/1). The

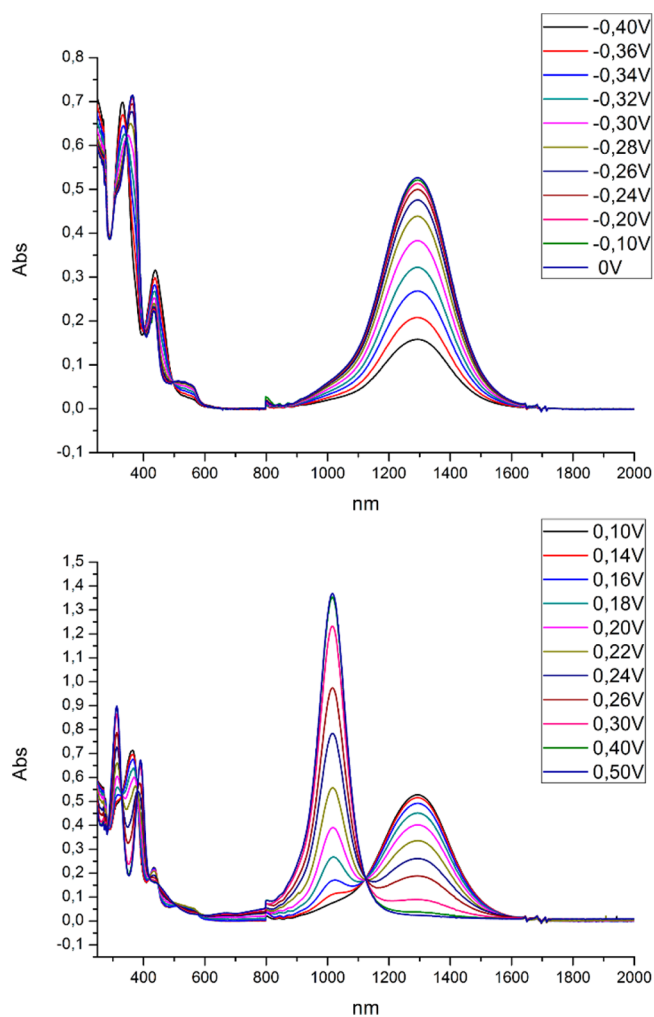


Figure 2. UV-vis-NIR monitoring of the electrochemical oxidation of $[\text{PPh}_4]_2[\text{Ni}(\text{Et-thiazdt})_2]$ in CH_2Cl_2 with $[\text{NBu}_4][\text{PF}_6]$ 0.2 M as electrolyte from -0.4 to 0.0 V (top) and from 0.1 to 0.5 V (bottom).

structure of the three species, **2**, **4**, and **5** were determined by single-crystal X-ray diffraction. As shown in Figures 3 and 4, the

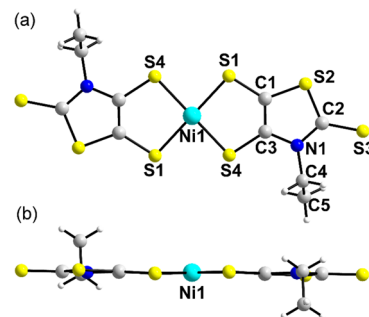


Figure 3. Top (a) and side (b) view of the molecular structure of $[\text{Ni}(\text{Et-thiazdt})_2]^{2-}$ in **2**.

$[\text{Ni}(\text{Et-thiazdt})_2]$ complex in its dianionic, monoanionic, and neutral state exhibits very similar geometry, with a square planar environment around the Ni atom, an almost planar structure, and a *trans* configuration of the two N-Et moieties. Note that the same *trans* geometry was also observed in the analogous gold complexes, $[\text{Au}(\text{Et-thiazdt})_2]^{-1,0,9}$ and for the dianionic $[\text{Ni}(\text{Me-thiazdt})_2]$ complex⁸ but in sharp contrast

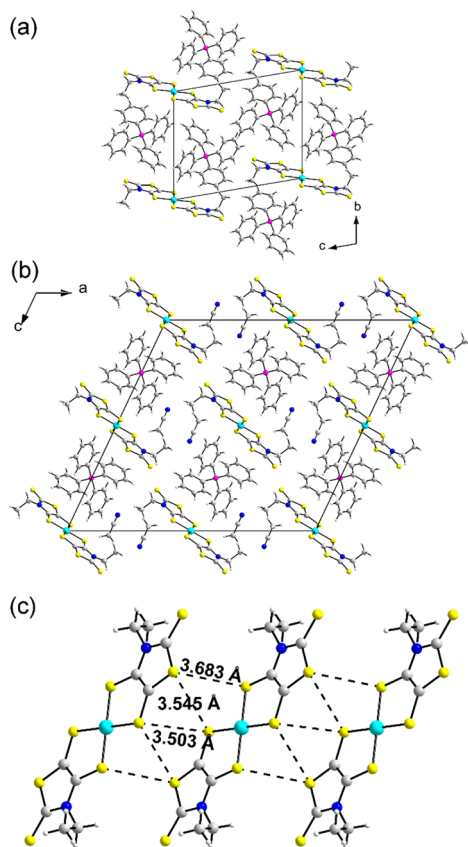


Figure 4. (a) Projection view along the *a* axis of the unit cell of $[\text{PPh}_4]_2[\text{Ni}(\text{Et-thiazdt})_2]$ (**2**). (b) Projection view along the *b* axis of the unit cell of $[\text{PPh}_4][\text{Ni}(\text{Et-thiazdt})_2]$ (**4**). (c) A detail of the chain of radical anion complexes $[\text{Ni}(\text{Et-thiazdt})_2]^{\bullet-}$ in **4**.

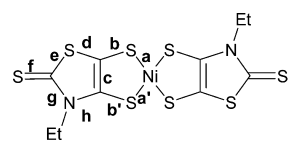
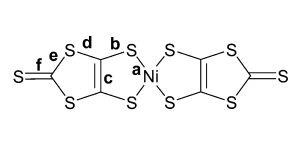
with that obtained with the radical anion where a mixture of *cis* and *trans* isomers was identified in the crystal structure of the

monoanionic $[\text{Ni}(\text{Me-thiazdt})_2]^{-1}$.⁸ Comparison of the intramolecular bond lengths within the three complexes $[\text{Ni}(\text{Et-thiazdt})_2]^n$, $n = -2, -1, 0$ (Table 2) highlights the evolution of the geometrical characteristics depending on the redox states of the complex.¹⁴ These bond length modifications occur essentially on the metallacycle rings with, upon oxidation of the dithiolate ligand, a lengthening of the C=C bond and a shortening of the Ni–S and S–C bonds, in accordance the oxidation of the ligand toward a dithioketonic structure. It is worth comparing these bond lengths values with those obtained for the $[\text{Ni}(\text{dmit})_2]^n$ analogues with $n = -2$,¹⁵ -1 ,¹⁶ and 0 .¹⁷ Within this series, the variation of the bond lengths on the metallacycle are essentially of the same order of magnitude than in $[\text{Ni}(\text{Et-thiazdt})_2]^n$, apart the C=C bond length in $[\text{Ni}(\text{dmit})_2]$, which is less affected when n varies from -2 to 0 . Otherwise the exocyclic C=S bonds face the same variation in both series with a shortening of the C=S bond length when n varies from -2 to 0 .

In the solid state, the dianionic salt **2** (Figure 4a) shows an alternation of the $[\text{Ni}(\text{Et-thiazdt})_2]^{2-}$ complex located on inversion center, with PPh_4^+ cations, in a general position giving rise to twin chains running along *a*. The cations are associated two-by-two through inversion centers into a so-called parallel quadruple phenyl embrace motif, while they interact with neighboring molecules within chains running along *a* with the translational quadruple phenyl embrace.¹⁸

The solid-state organization of the monoanionic salt requires a deeper investigation as the paramagnetic anion's organization will control the solid-state magnetic properties of the $[\text{PPh}_4][\text{Ni}(\text{Et-thiazdt})_2]$ salt **4**. The salt crystallizes with the $[\text{Ni}(\text{Et-thiazdt})_2]^{1-}$ complex located on an inversion center, the PPh_4^+ cation on a 2-fold axis, together with a CH_3CN molecule in general position, hence the formulation $[\text{PPh}_4][\text{Ni}(\text{Et-thiazdt})_2] \cdot (\text{CH}_3\text{CN})_2$. In the solid state (Figure 4b), the paramagnetic $[\text{Ni}(\text{Et-thiazdt})_2]^{1-}$ complexes are isolated from each other in the *ac* plane by the PPh_4^+ counterion, whereas

Table 2. Intramolecular Bond Lengths (in Å) in Dianionic **2**, Monoanionic **4**, and Neutral **5** $[\text{Ni}(\text{Et-thiazdt})_2]^n$ Species Together with Those of the $[\text{Ni}(\text{dmit})_2]^n$, $n = -2, -1, 0$

<i>n</i>	$[\text{Ni}(\text{Et-thiazdt})_2]^n$			$[\text{Ni}(\text{dmit})_2]^n$		
	-2	-1	0	-2	-1	0
<i>a</i>	2.2060(7)	2.1778(6)	2.1580(6)	2.188(0)	2.151(3)	2.144(2)
<i>a'</i>	2.1983(8)	2.1560(6)	2.1577(6)	2.192(1)	2.160(3)	2.150(2)
<i>b</i>	1.735(2)	1.722(2)	1.685(2)	1.749(0)	1.72(1)	1.699(7)
<i>b'</i>	1.741(2)	1.712(2)	1.700(2)	1.735(1)	1.73(1)	1.698(7)
<i>c</i>	1.338(3)	1.356(3)	1.388(3)	1.342(1)	1.35(1)	1.391(9)
<i>d</i>	1.751(2)	1.739(2)	1.733(2)	1.730(1)	1.73(1)	1.731(7)
<i>e</i>	1.732(3)	1.735(3)	1.755(2)	1.744(1)	1.72(1)	1.732(7)
<i>f</i>	1.692(2)	1.664(3)	1.640(2)	1.733(0)	1.732(1)	1.757(8)
<i>g</i>	1.353(3)	1.362(4)	1.372(3)	1.732(1)	1.64(1)	1.742(7)
<i>h</i>	1.409(3)	1.398(3)	1.378(3)	1.640(1)	1.62(1)	1.625(8)

short lateral S⋯S intermolecular contacts can be observed along the *b* axis. These S⋯S contacts between neighboring complexes, notably shorter than the sum of the van der Waals radii are detailed in Figure 4c, and these could give rise to a uniform spin chain behavior. Temperature dependence of the magnetic susceptibility (Figure 5) shows actually a behavior

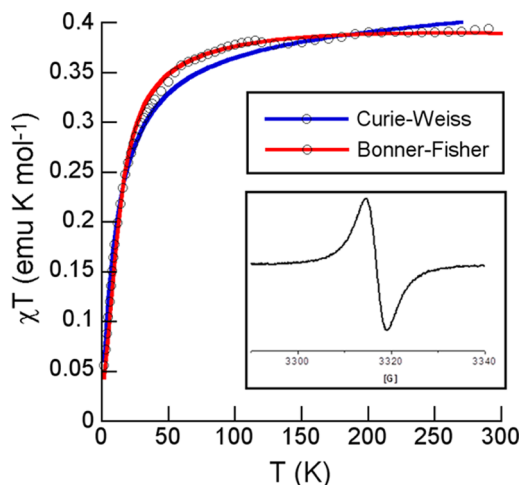


Figure 5. Temperature dependence of the χT product for the monoanionic paramagnetic salt $[\text{PPh}_4][\text{Ni}(\text{Et-thiazdt})_2]$ (**4**). Inset: EPR spectrum of **4** in CH_2Cl_2 solution at 300 K.

close to a Curie–Weiss law. Considering a *g* value of 2.006 usually found in such Ni dithiolene complexes, a better fit is indeed obtained with a uniform spin chain model (Bonner–Fisher),¹⁹ with an added Curie tail contribution, giving a *J/k* value for the spin chain of $-16.1(7)$ K,²⁰ together with 5, 9% Curie-type defaults. The solution EPR spectra of salt **4** in CH_2Cl_2 measured at 300 K and in frozen solution display an isotropic signal at $g_{\text{iso}} = 2.041$ (300 K), with no hyperfine coupling resolved. This *g* value and weak anisotropy compare with those reported for other anionic nickel dithiolene complexes²¹ where the spin density is strongly delocalized within the two metallacycles.

It is also worth analyzing the solid-state organization of the neutral complex **5**, particularly to compare it with that of the radical gold dithiolene analogue $[\text{Au}(\text{Et-thiazdt})_2]^{\bullet}$ described earlier.⁹ The neutral Ni complex crystallizes in the monoclinic system, space group $P2_1/a$, with the complex on an inversion center. It is not isostructural with the analogous gold complex. In the solid state, the molecules form uniform stacks along *a* axis with a mean plane to plane distance of 3.54 Å (Figure 6). An important difference between the structures of the nickel and gold complexes is found in the overlap pattern between molecules within the stacks. As shown in Figure 7, this overlap shows a large longitudinal offset in the nickel complex while a small lateral offset was present in the gold complex. We also note that in **5**, the nickel atom lies directly above the smaller nitrogen atom, whereas in the gold complex, the overlap between the central part of the complex is preferred.

This situation is at first sight surprising as, among the few neutral bis(dithiolene) complexes which have been described to date with *both* nickel and gold, the majority is found with very similar structures with nickel and gold, which one could indeed anticipate from their very similar shape. We have collected in Table 3 and Figure 8 these pairs of complexes with some details about their solid-state arrangement. It appears that isostructural

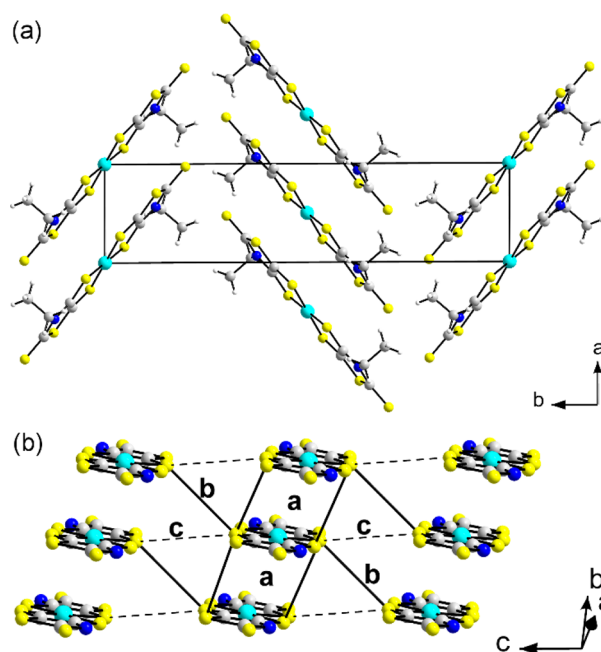


Figure 6. (a) Projection view along *c* of the unit cell of **5**. (b) Detail of one (a,c) layer, viewed along the long molecular axis, with black and dotted lines indicating the shortest S⋯S contacts between neighboring molecules.

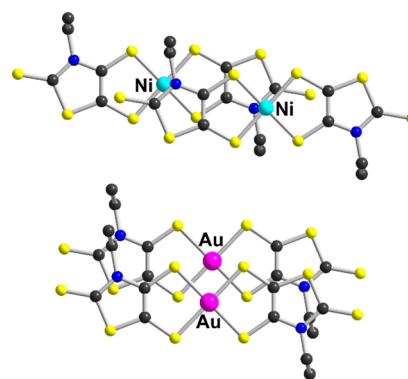


Figure 7. Projection view, perpendicular to the molecular planes, of the overlap between neighboring molecules in the two neutral complexes. Top: the closed-shell $[\text{Ni}(\text{Et-thiazdt})_2]^0$ Bottom: the radical $[\text{Au}(\text{Et-thiazdt})_2]^{\bullet}$.

pairs are actually found in those systems with bulky dithiolene ligands, which hinder a close face-to-face association of the complexes. With complexes able to stack on top of each other (with dddt, bdt, Et-thiazdt ligands), the recurrent face-to-face organization of the complexes differs actually depending on the metal nature, with shorter plane-to-plane distances and smaller deviations from an eclipsed overlap in the gold complexes. These features are correlated to the radical nature of the gold dithiolene complexes, whose π -type SOMO is essentially localized on the $[\text{Au}(\text{S}_2\text{C}_2)_2]$ metallacycles.²² Accordingly, their stabilization through overlap interaction—into pairs or in infinite stacks—favors short intermolecular contacts between the central parts of the complexes, although the structures of the corresponding nickel complexes lacking this extra electron are controlled exclusively by nonbonding intermolecular interactions. Similar effects of overlap interactions are recurrently observed within organic radical dimers or

Table 3. Comparison of the Structural Characteristics of Neutral Nickel and Gold Dithiolene Complexes^a

complex	[Ni(dt) ₂] ⁰	isostructural	[Au(dt) ₂] [•]	ref Ni	ref Au
nonhindered complexes					
[M(ddd) ₂]	face to face assoc. longitudinal shift plane-to-plane: 3.75 Å	no	face to face assoc. longitudinal shift plane-to-plane: 3.58 Å	29	30
[M(bdt) ₂]			face to face assoc. small lateral shift plane-to-plane: 3.57 Å		31
[M(Et-thiazdt) ₂]	face to face assoc. longitudinal shift (Figure 7b) plane-to-plane: 3.55 Å	no	face to face assoc. lateral shift (see Figure 7a) plane-to-plane: 3.57 Å	this work	9
[M(F ₂ pdt) ₂]	face to face assoc. fluorine segregation plane-to-plane: 3.86 Å	yes	face to face assoc. fluorine segregation plane-to-plane: 3.54 Å	32	32
hindered complexes					
[M(DL-bordt) ₂]	strong steric hindrance weak lateral interactions	yes	strong steric hindrance weak lateral interactions	33	33
[M(S ₂ C ₂ Ph ₂) ₂]	phenyl out of plane large lateral shift plane-to-plane: 3.80 Å	yes	phenyl out of plane large lateral shift plane-to-plane: 3.87 Å	34	35
[M(S ₂ C ₂ (OC ₄) ₂)]	phenyl out of plane large lateral shift plane-to-plane: 3.63 Å	yes	phenyl out of plane large lateral shift plane-to-plane: 3.62 Å	36	36

^aSee Figure 8 for the dithiolene abbreviations.

stacks,^{23,24} and provide the elementary building blocks for organic conductors based on cation or anion radical salts. In these organic salts, however, the comparison of the solid-state structure with analogous, nonradical systems is not possible, at variance with the series of neutral nickel and gold dithiolene complexes described here. In that respect, the comparison of the face-to-face organization of the radical [Au(Et-thiazdt)₂][•] and the diamagnetic [Ni(Et-thiazdt)₂]⁰ shown here in Figure 7 is particularly enlightening. Note also that such a comparison between neutral nickel and gold dithiolene complexes can be also made on the tetrathiafulvalenedithiolate complexes described by Kobayashi et al. (Chart 2). Although the trimethylene derivatives [Ni(tmdt)₂] and [Au(tmdt)₂],^{25,26} which adopt a tight three-dimensional structure, are actually isostructural, the other reported complexes with two trifluoromethyl groups in [M(hfdt)₂],²⁷ or propylenedithio substituents in [M(ptdt)₂] (M = Au, Ni),²⁸ organize in layered, two-dimensional structures, and are not isostructural. In both series, the gold complexes are found indeed in almost eclipsed dimers, and the nickel complexes exhibit more regular stacks with larger longitudinal shifts, as found here in [M(thiazdt)₂]. It again illustrates the tendency of the gold dithiolene complexes, with a spin density concentrated on the two metallacycles, to associate into eclipsed dimers.

Because of their closed shell nature, such simple neutral Ni dithiolene complexes are expected to be essentially insulating.³⁷ However, the large size of the crystals grown by electrocrystallization³⁸ leads us to infer that [Ni(Et-thiazdt)₂] **5** could be more conducting than anticipated. Accordingly, resistivity measurements were performed on single crystals along the *a* stacking direction (axis of the needle). The room-temperature

conductivity at ambient pressure, σ_{RT} (1 bar) is around $0.014 \pm 0.005 \text{ S cm}^{-1}$ (considering the error made in measuring the section of the needles). This conductivity is rather high and unexpected considering that it was measured on neutral closed-shell species. Indeed, except for the metallic and superconducting Ni complexes with two tetrathiafulvalene dithiolate ligands reported by Kobayashi et al.,^{25–28,39} one single example of conductivity measured on single crystals has been reported for the neutral [Ni(dmit)₂] which exhibits a lower conductivity under ambient conditions of $\sigma = 3.5 \times 10^{-3} \text{ S cm}^{-1}$.¹⁷ Note that under very high pressure (above 15.9 GPa) [Ni(dmit)₂] has been recently reported to become metallic.⁴⁰ As presented in Figure 9, the temperature dependence of the conductivity shows a semiconducting behavior with a rather small activation energy $E_a = 2370 \text{ K}$ (0.20 eV), as deduced from the fit of the data with a law of the type $\sigma = \sigma_0 \exp(-E_a/kT)$. The evolution of the room-temperature conductivity with pressure (see inset of Figure 9) was found to be nearly exponential up to 12 kbar in agreement with a semiconducting character. Actually, the activation energy is only slightly reduced under a pressure of 12 kbar, $E_a = 1980 \text{ K}$ (0.17 eV).

Band structure calculations for [Ni(Et-thiazdt)₂] **5** were performed in the extended Hückel frame. The $\beta_{\text{HOMO-HOMO}}$ interaction energies amount, in absolute value, to 0.2253, 0.0233, and 0.0085 eV for, respectively, the intermolecular interactions noted as a, b, c in Figure 6b, demonstrating the strong one-dimensional character of the complex. The calculated band structure (Figure 10) confirms the presence of a gap between valence band (HOMO) and conduction band (LUMO) with a direct gap at M point of 0.55 eV, whereas the indirect gap ($\Gamma \rightarrow M$) decreases to 0.09 eV.

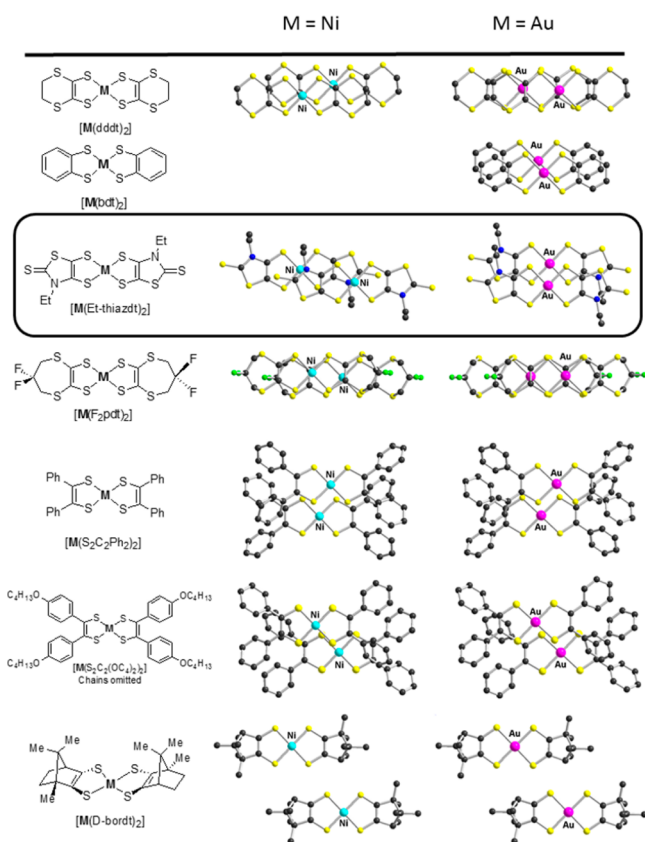
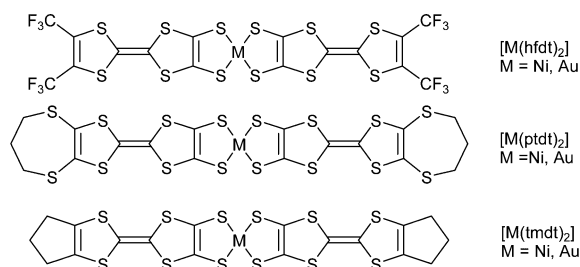


Figure 8. Detail of the overlap patterns between $[M(\text{dithiolene})_2]$ complexes, with $M = \text{Ni}$ or Au .

Chart 2



Note that the measured activation energy at ambient pressure (0.20 eV) corresponds actually to an intermediate gap value ($2 \times 0.20 = 0.40$ eV), close to the calculated direct gap. On the basis of this band structure and the small indirect gap, one might also expect that larger band dispersions for both HOMO and LUMO bands would eventually allow for a band overlap and associated metallic character. We have seen that pressure application, at least up to 12 kbar was not sufficient for that purpose. Measurements under higher pressures should be considered, as recently demonstrated on $[\text{Ni}(\text{dmit})_2]$,⁴⁰ together with the preparation of the diselenolate analogues. We have noticed indeed in the series of gold dithiolene complexes that the S/Se substitution was an efficient way to close such gaps.¹⁰ These combined physical and chemical pressure effects are currently being explored.

EXPERIMENTAL SECTION

General. NMR spectra were recorded on a Bruker AV300III spectrometer at room temperature using perdeuterated solvents.

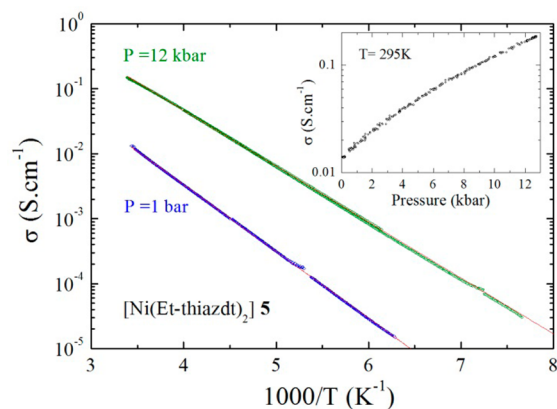


Figure 9. (a) Electrical conductivity data of $[\text{Ni}(\text{Et-thiazdt})_2]$ 5 along a axis at ambient pressure and 12 kbar plotted as $\log \sigma$ versus the inverse temperature. The red lines are a linear fit of the data giving the activation energies of 0.20 eV at 1 bar and 0.17 eV at 12 kbar. (Inset) Pressure dependence of the conductivity of $[\text{Ni}(\text{Et-thiazdt})_2]$ 5 at room temperature. Note the log scale for the conductivity axis.

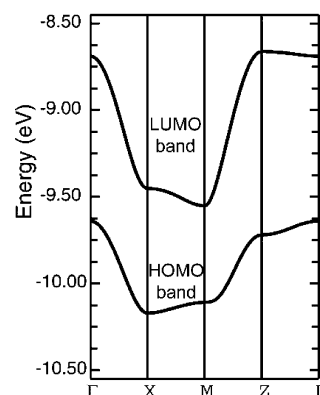


Figure 10. Calculated band structure for $[\text{Ni}(\text{Et-thiazdt})_2]$ 5.

Chemical shifts are reported in ppm referenced to TMS for ¹H NMR. Mass spectra were recorded with Bruker MicrOTOF-Q II instrument for complex 2, and with Thermo-fisher Q-Exactive instrument for complex 4 by the Centre Régional de Mesures Physiques de l'Ouest, Rennes. CVs were carried out on a 10^{-3} M solution of complex in CH_2Cl_2 - $[\text{NBu}_4][\text{PF}_6]$ 0.1 M. The spectroelectrochemical setup was performed in CH_2Cl_2 - $[\text{NBu}_4][\text{PF}_6]$ 0.2 M. A Cary 5 spectrophotometer was employed to record the UV-vis-NIR spectra. CVs were recorded on a Model 362 scanning potentiostat from EG&G Instruments at 0.1 V s^{-1} on a platinum disk electrode (1 mm^2). Potentials were measured versus KCl Saturated Calomel Electrode (SCE). EPR spectra were performed on a Bruker ESP-300 spectrometer. Silica gel used in chromatographic separations was obtained from Acros Organics (Silica Gel, ultra pure, $40\text{--}60 \mu\text{m}$). All other reagents and materials from commercial sources were used without further purification.

Synthesis of $[\text{PPh}_4]_2[\text{Ni}(\text{Et-thiazdt})_2]$ 2 Starting from 1. Under inert atmosphere at 0°C , LDA was prepared by adding BuLi (3.56 mL, 5.7 mmol, 1.6 M in hexanes) to a solution of diisopropylamine (0.8 mL, 5.7 mmol) in 15 mL of anhydrous THF. The LDA solution was then added to a solution of 1,3-thiazoline-2-thione 1 (0.55 g, 3.8 mmol) in 50 mL of anhydrous THF at -10°C . After stirring for 30 min, sulfur (183 mg, 5.7 mmol) was added to the reaction mixture, and the medium was stirred for an additional 30 min before the addition of LDA (7.6 mmol prepared from 4.75 mL of BuLi and 1.08 mL of diisopropylamine). The reaction mixture was stirred for 3 h, and sulfur was added (244 mg, 7.6 mmol) followed 30 min later by the addition of $\text{NiCl}_2 \cdot 6\text{H}_2\text{O}$ (0.45 g, 1.9 mmol) and PPh_4Cl (1.42 g, 3.8 mmol). Then the temperature was allowed to rise to room

Table 4. Crystallographic Data

	2	4	5
formulas	C ₅₈ H ₅₀ N ₂ NiP ₂ S ₈	C ₃₈ H ₃₆ N ₄ NiPS ₈	C ₁₀ H ₁₀ N ₂ NiS ₈
fw (g mol ⁻¹)	1150.1	894.93	473.39
system	triclinic	monoclinic	monoclinic
space group	$P\bar{1}$	C2/c	P2 ₁ /a
a (Å)	7.4923(15)	26.2864(15)	5.6672(2)
b (Å)	12.525(3)	7.1977(4)	21.7434(7)
c (Å)	14.916(4)	24.6704(15)	7.3720(2)
α (deg)	98.28(2)	90	90
β (deg)	96.835(19)	115.314(2)	110.885(2)
γ (deg)	96.802(18)	90	90
V (Å ³)	1350.1(5)	4219.5(4)	848.72(5)
T (K)	298	150(2)	293(2)
Z	1	4	2
D _{calc} (g cm ⁻³)	1.417	1.409	1.852
μ (mm ⁻¹)	0.769	0.927	2.118
total reflns	30652	17697	17686
abs corr	multiscan	multiscan	multiscan
unique reflns (R _{int})	6220	4844 (0.0373)	1943 (0.0331)
unique reflns (I > 2σ(I))	6204	3932	1565
R ₁ , wR ₂	0.0385, 0.0805	0.0353, 0.0945	0.0306, 0.0618
R ₁ , wR ₂ (all data)	0.0613, 0.0907	0.0540, 0.1195	0.0442, 0.0644
GOF	1.071	1.195	1.089

temperature and the reaction mixture was stirred for 15 h. Thereafter the mixture was filtered, washed with ethanol and dried under vacuum. The resulting solid is recrystallized with acetonitrile to afford complex 2 as dark red crystals in 17% yield ($m = 0.37$ g).

Synthesis of [PPh₄]₂[Ni(Et-thiazdt)₂] 2 Starting from 3. To a dry two-neck flask containing 3 (0.4 g, 1.27 mmol), 10 mL of 1 M NaOMe in MeOH was added under nitrogen at room temperature. After stirring for 30 min, a solution containing NiCl₂ (98.8 mg, 0.76 mmol) in 4 mL of dried MeOH was added to the reaction mixture followed, 5 h later, by the addition of PPh₄Cl (0.71 g, 1.91 mmol) in 4 mL of dried MeOH. The reaction mixture was stirred for 15 h. The dianionic complex 2 precipitated out and was isolated by filtration to afford 2 in 52% yield, mp 202 °C. ¹H NMR (CDCl₃, 300 MHz) δ: 1.24 (t, 6H, 2CH₃, ³J_{HH} = 7.0 Hz), 3.48 (q, 4H, 2CH₂, ³J_{HH} = 7.0 Hz), 7.69–7.78 (m, 40H, H_A). ¹³C NMR (CDCl₃, 75 MHz) δ: 12.8 (CH₃), 42.9 (CH₂), 116.9 (C=C), 118.1 (C=C), 130.7 (CHAr), 134.5 (CHAr), 135.6 (CHAr), 200.3 (C=S); HRMS (ESI) *m/z*: calcd for C₅₈H₅₀N₂⁵⁸NiP₂S₈ [2C⁺, A⁻]⁺, 1150.0563; found, 1150.0565.

Synthesis of [PPh₄]₂[Ni(Et-thiazdt)₂] 4. Under inert atmosphere, [Cp₂Fe][PF₆]₂ (30 mg, 0.09 mmol) was dissolved in 10 mL of distilled dichloromethane, and [PPh₄]₂[Ni(R-thiazdt)₂] (100 mg, 0.09 mmol) was added to the reaction medium. After stirring for 1 h, pentane (40 mL) was added, and the precipitate was filtered. Complex 4 was recrystallized with a solution of toluene/acetonitrile (1:1) to afford the title complex as dark red crystals in 71% yield ($m = 0.05$ g), mp 204 °C. HRMS (ESI) *m/z*: calcd for ion C₁₀H₁₀N₂NiS₈⁻, 471.7969; found, 471.7967. Anal. Calcd for C₃₄H₃₀N₂NiPS₈: C, 50.24; H, 3.72; N, 3.45. Found: C, 50.66; H, 3.72; N, 3.29.

Synthesis of [Ni(Et-thiazdt)₂] 5. In a two-compartment cell equipped with Pt electrodes (diameter 1 mm, length 2 cm) NET₄Br (210 mg, 1 mmol) dissolved in 16 mL of CH₃CN was introduced in both compartment as supporting electrolyte. The nickel complex 4 (8 mg, 1.69 × 10⁻² mmol) was introduced in the anodic compartment. The current intensity was adjusted to 0.4 μA, and the reaction was left during 5 days. Crystals of the neutral Ni complex 5 were collected on the anode. Anal. Calcd for C₁₀H₁₀N₂NiS₈: C, 25.37; H, 2.13; N, 5.92; S, 54.18. Found: C, 25.45; H, 2.00; N, 5.69; S, 54.66.

X-ray Crystallography. Details of the structural analyses for 2, 4, and 5 are summarized in Table 4. X-ray crystal structure determinations were performed on an APEXII Bruker-AXS diffractometer equipped with a CCD camera and a graphite-monochromated

Mo Kα radiation source ($\lambda = 0.71073$ Å), from the Centre de Diffractométrie (CDIFX), Université de Rennes 1, France. Structures were solved by direct methods using the SIR97 program,⁴¹ and then refined with full-matrix least-squares methods based on F² (SHELXL-97)⁴² with the aid of the WINGX program.⁴³ All non-hydrogen atoms were refined with anisotropic atomic displacement parameters. H atoms were finally included in their calculated positions.

Resistivity Measurements. The resistivity measurements were performed in four points along the long axis of the needles (*a* crystallographic axis) using a dc current in the range of $I_{dc} = 0.1–1$ μA. Gold pads have been previously evaporated on the surface of the crystals in order to improve the quality of the contacts and gold wires (17 μm in diameter) were attached to these pads with silver paint. Hydrostatic pressure was applied at room temperature in a CuBe clamp cell using Daphne 7373 silicone oil as the pressure transmitting medium. The pressure was determined, at room temperature, using a manganin resistance gauge located in the pressure cell close to the sample. The pressures indicated here are room-temperature values and the loss of pressure occurring during cooling is estimated to 1.5 kbar starting from 12 kbar. Variable temperature data have been provided by a homemade cryostat equipped with a 4K pulse-tube for the ambient pressure experiment, using a cernox thermometer and by a cryocooler equipment for the measurement under high pressure, using a copper-constantan thermocouple located inside the pressure cell as a thermometer.

Band Structure Calculations. The tight-binding band structure calculations and β_{HOMO–HOMO} interaction energies were based upon the effective one-electron Hamiltonian of the extended Hückel method,⁴⁴ as implemented in the Caesar 1.0 chain of programs.⁴⁵ The off-diagonal matrix elements of the Hamiltonian were calculated according to the modified Wolfsberg–Helmholz formula.⁴⁶ All valence electrons were explicitly taken into account in the calculations and the basis set consisted of double-ζ Slater-type orbitals for all atoms except H single-ζ Slater-type orbitals for H. The exponents, contraction coefficients, and atomic parameters are detailed below. S(3s): –20.0, 2.662, 0.5564, 1.688, 0.48743. S(3p): –13.3, 2.328, 0.5208, 1.333, 0.5439. C(2s): –21.4, 1.831, 0.7616, 1.153, 0.2630. C(2p): –11.4, 2.730, 0.25946, 1.257, 0.80264. Ni(4s): –9.70, 2.10, 1.0. Ni(4p): –5.15, 2.10, 1.0. Ni(3d): –13.49, 5.75, 0.5798, 2.30, 0.5782. N(2s): –26.0, 2.261, 0.7297, 1.424, 0.3455. N(2p): –13.4, 3.249, 0.2881, 1.499, 0.7783. H(1s): –13.6, 1.3, 1.0.

■ ASSOCIATED CONTENT

S Supporting Information

X-ray crystallographic files in CIF format. This material is available free of charge via the Internet at <http://pubs.acs.org>.

■ AUTHOR INFORMATION

Corresponding Author

*E-mail: Dominique.lorcy@univ-rennes1.fr.

Notes

The authors declare no competing financial interest.

■ ACKNOWLEDGMENTS

We thank the CDIFX (Rennes) for access to the X-ray diffraction facilities and the ANR (France) for financial support through project no. 12-BS07-0032. We wish to thank Thierry Guizouarn for the magnetic measurements.

■ REFERENCES

- (1) (a) Kato, R. *Bull. Chem. Soc. Jpn.* **2014**, *87*, 355–374. (b) Kato, R. *Chem. Rev.* **2004**, *104*, 5319–5346.
- (2) *Dithiolene Chemistry: Synthesis, Properties, and Applications*; Karlin, K. D., Stiefel, E. I., Eds.; Wiley: New York, 2004; Vol. 52.
- (3) (a) Cassoux, P.; Valade, L.; Kobayashi, H.; Kobayashi, A.; Clark, R. A.; Underhill, A. E. *Coord. Chem. Rev.* **1991**, *110*, 115–160. (b) Olk, R.-M.; Olk, B.; Dietzsch, W.; Kirmse, R.; Hoyer, E. *Coord. Chem. Rev.* **1992**, *117*, 99–131. (c) Cassoux, P. *Coord. Chem. Rev.* **1999**, *185*–186, 213–232. (d) Pullen, A. E.; Olk, R.-M. *Coord. Chem. Rev.* **1999**, *188*, 211–262. (e) Robertson, N.; Cronin, L. *Coord. Chem. Rev.* **2002**, *227*, 93–127.
- (4) Zanello, P.; Grigiotti, E. In *Trends in Molecular Electrochemistry*; Pombeiro, A. J. L., Amatore, C., Eds.; Fontis Media and Marcel Dekker Inc: New York, 2004; Chapter 1, pp 3–70.
- (5) Mueller-Westerhoff, U. T.; Vance, B. In *Comprehensive Coordination Chemistry*; Wilkinson, G., Gillard, R. D., McCleverty, J. A., Eds.; Pergamon Press: Oxford, U.K., 1987.
- (6) (a) Bigoli, F.; Deplano, P.; Devillanova, F. A.; Lippolis, V.; Lukes, P. J.; Mercuri, M. L.; Pellinghelli, M. A.; Trogu, E. F. *J. Chem. Soc., Chem. Commun.* **1995**, 371–372. (b) Bigoli, F.; Deplano, P.; Devillanova, F. A.; Ferraro, J. R.; Lippolis, V.; Lukes, P. J.; Mercuri, M. L.; Pellinghelli, M. A.; Trogu, E. F.; Williams, J. M. *Inorg. Chem.* **1997**, *36*, 1218–1226. (c) Bigoli, F.; Deplano, P.; Mercuri, M. L.; Pellinghelli, M. A.; Pintus, G.; Trogu, E. F.; Zonnebda, G.; Wang, H. H.; Williams, J. M. *Inorg. Chim. Acta* **1998**, *273*, 175–183. (d) Aragoni, M. C.; Arca, M.; Demartin, F.; Devillanova, F. A.; Garau, A.; Isaia, F.; Lejl, F.; Lippolis, V.; Verani, G. *J. Am. Chem. Soc.* **1999**, *121*, 7098–7107.
- (7) Aragoni, M. C.; Arca, M.; Devillanova, F. A.; Isaia, F.; Lippolis, V.; Mancini, A.; Pala, L.; Slawin, A. M. Z.; Woollins, J. D. *Inorg. Chem.* **2005**, *44*, 9610–9612.
- (8) Eid, S.; Fourmigué, M.; Roisnel, T.; Lorcy, D. *Inorg. Chem.* **2007**, *46*, 10647–10654.
- (9) Tenn, N.; Bellec, N.; Jeannin, O.; Piekara-Sady, L.; Auban-Senzier, P.; Iniguez, J.; Canadell, E.; Lorcy, D. *J. Am. Chem. Soc.* **2009**, *131*, 16961–16967.
- (10) Yzambart, G.; Bellec, N.; Nasser, G.; Jeannin, O.; Roisnel, T.; Fourmigué, M.; Auban-Senzier, P.; Iniguez, J.; Canadell, E.; Lorcy, D. *J. Am. Chem. Soc.* **2012**, *134*, 17138–17148.
- (11) Olk, R.-M.; Röhr, A.; Sieler, J.; Köhler, K.; Kirmse, R.; Dietzsch, W.; Hoyer, E.; Olk, B. *Z. Anorg. Allg. Chem.* **1989**, *577*, 206–216.
- (12) Arca, M.; Demartin, F.; Devillanova, F. A.; Garau, A.; Isaia, F.; Lejl, F.; Lippolis, V.; Pedraglio, S.; Verani, G. *J. Chem. Soc., Dalton Trans.* **1998**, 3731–3736.
- (13) Perochon, R.; Poriel, C.; Jeannin, O.; Piekara-Sady, L.; Fourmigué, M. *Eur. J. Inorg. Chem.* **2009**, 5413–5421.
- (14) (a) Lim, B. S.; Fomitchev, D. V.; Holm, R. H. *Inorg. Chem.* **2001**, *40*, 4257–4262. (b) Ray, K.; Weyhermüller, T.; Neese, F.; Wieghardt, K. *Inorg. Chem.* **2005**, *44*, 5345–5360.
- (15) Marsh, R. E. *Acta Crystallogr., Sect. B: Struct. Sci.* **2009**, *65*, 782–783.
- (16) Lindqvist, O.; Andersen, L.; Sieler, J.; Steimecke, G.; Hoyer, E. *Acta Chem. Scand., Ser. A* **1982**, *36*, 855–856.
- (17) Valade, L.; Legros, J. P.; Bousseau, M.; Cassoux, P.; Garbauskas, M.; Interrante, L. V. *J. Chem. Soc., Dalton Trans.* **1985**, 783–794.
- (18) Dance, I.; Scudder, M. *Chem.—Eur. J.* **1996**, *2*, 481–486.
- (19) Bonner, J. C.; Fisher, M. E. *Phys. Rev.* **1964**, *135*, A640–A658.
- (20) The associated spin Hamiltonian reads as $H = 2J S SiSi + I$. See *Molecular Magnetism*; Kahn, O., Ed.; VCH: New York, 1993.
- (21) Kisch, H.; Eisen, B.; Dinnebier, R.; Shankland, K.; David, W. I. F.; Knoch, F. *Chem.—Eur. J.* **2001**, *7*, 738–748.
- (22) Kokatam, S.; Ray, K.; Pap, J.; Bill, E.; Geiger, W. E.; LeSuer, R. J.; Rieger, P. H.; Weyhermüller, T.; Neese, F.; Wieghardt, K. *Inorg. Chem.* **2007**, *46*, 1100–1111.
- (23) Fourmigué, M. In *The Importance of p-Interactions in Crystal Engineering*; John Wiley & Sons, Ltd.: Chichester, West Sussex, U.K., 2012; Chapter 6, pp 143–162.
- (24) Devic, T.; Yuan, M.; Adams, J.; Frederickson, D. C.; Lee, S.; Venkataraman, D. *J. Am. Chem. Soc.* **2005**, *127*, 14616–14627.
- (25) Tanaka, H.; Okano, Y.; Kobayashi, H.; Suzuki, W.; Kobayashi, A. *Science* **2001**, *291*, 285–287.
- (26) Suzuki, W.; Fujiwara, E.; Kobayashi, A.; Fujishiro, Y.; Nishibori, E.; Takata, M.; Sakata, M.; Fujiwara, H.; Kobayashi, H. *J. Am. Chem. Soc.* **2003**, *125*, 1486–1487.
- (27) Sasa, M.; Fujiwara, E.; Kobayashi, A.; Ishibashi, S.; Terakura, K.; Okano, Y.; Fujiwara, H.; Kobayashi, H. *J. Mater. Chem.* **2005**, *15*, 155–163.
- (28) (a) Zhou, B.; Yajima, H.; Idobata, Y.; Kobayashi, A.; Kobayashi, T.; Nishibori, E.; Sawa, H.; Kobayashi, H. *Chem. Lett.* **2012**, *41*, 154–156. (b) Kobayashi, A.; Tanaka, H.; Kumasaki, M.; Torii, H.; Narymbetov, B.; Adachi, T. *J. Am. Chem. Soc.* **1999**, *121*, 10763–10771.
- (29) (a) Kim, H.; Kobayashi, A.; Sasaki, Y.; Kato, R.; Kobayashi, H. *Bull. Chem. Soc. Jpn.* **1988**, *61*, 579. (b) Nagapeytan, S. S.; Shklover, V. E.; Vetoshkina, L. V.; Kotov, A. I.; Ukhin, L. Y.; Struchkov, Y. T.; Yagubskii, E. B. *Mater. Sci.* **1988**, *14*, 5–9.
- (30) Schultz, A. J.; Wang, H. H.; Soderholm, L. C.; Sifter, T. L.; Williams, J. M.; Bechgaard, K.; Whangbo, M.-H. *Inorg. Chem.* **1987**, *26*, 3757.
- (31) Rindorf, G.; Thorup, N.; Bjørnholm, T.; Bechgaard, K. *Acta Crystallogr., Sect. C: Cryst. Struct. Commun.* **1990**, *46*, 1437.
- (32) Dautel, O. J.; Fourmigué, M.; Canadell, E.; Auban-Senzier, P. *Adv. Funct. Mater.* **2002**, *12*, 693.
- (33) Perochon, R.; Poriel, C.; Jeannin, O.; Piekara-Sady, L.; Fourmigué, M. *Eur. J. Inorg. Chem.* **2009**, 5413–5421.
- (34) (a) Megnamisi-Belombe, M.; Nuber, B. *Bull. Chem. Soc. Jpn.* **1989**, *62*, 4092–4094. (b) Miao, Q.; Gao, J.; Wang, Z.; Yu, H.; Luo, Y.; Ma, T. *Inorg. Chim. Acta* **2011**, *367*, 619–627.
- (35) Papavassiliou, G. C.; Anyfantis, G. C.; Raptopoulou, C. P.; Psycharis, V.; Ioannidis, N.; Petrouleas, V.; Paraskevopoulou, P. *Polyhedron* **2009**, *28*, 3368–3372.
- (36) Perochon, R.; Piekara-Sady, L.; Jurga, W.; Clérac, R.; Fourmigué, M. *Dalton Trans.* **2009**, 3052–3061.
- (37) Garreau-de Bonneval, B.; Moineau-Chane Ching, K. I.; Alary, F.; Bui, T.-T.; Valade, L. *Coord. Chem. Rev.* **2010**, *254*, 1457–1467.
- (38) Batail, P.; Boubekour, K.; Fourmigué, M.; Gabriel, J.-C. *P. Chem. Mater.* **1998**, *10*, 3005–3015.
- (39) (a) Cui, H.-B.; Kobayashi, H.; Ishibashi, S.; Sasa, M.; Iwase, F.; Kato, R.; Kobayashi, A. *J. Am. Chem. Soc.* **2014**, *136*, 7619–7622. (b) Cui, H.-B.; Brooks, J. S.; Kobayashi, A.; Kobayashi, H. *J. Am. Chem. Soc.* **2009**, *131*, 6358–6359.
- (40) Cui, H.-B.; Tsumuraya, T.; Miyazaki, T.; Okano, Y.; Kato, R. *Eur. J. Inorg. Chem.*, **2014**, in press. [org/10.1002/ejic.201400130](http://dx.doi.org/10.1002/ejic.201400130).

- (41) Altomare, A.; Burla, M. C.; Camalli, M.; Cascarano, G.; Giacovazzo, C.; Guagliardi, A.; Moliterni, A. G. G.; Polidori, G.; Spagna, R. *J. Appl. Crystallogr.* **1999**, *32*, 115–119.
- (42) Sheldrick, G. M. *Acta Crystallogr.* **2008**, *A64*, 112–122.
- (43) Farrugia, L. J. *J. Appl. Crystallogr.* **1999**, *32*, 837–838.
- (44) Whangbo, M.-H.; Hoffmann, R. *J. Am. Chem. Soc.* **1978**, *100*, 6093–6098.
- (45) Ren, J.; Liang, W.; Whangbo, M.-H. *Crystal and Electronic Structure Analysis Using CAESAR*; PrimeColor Software, Inc.: Cary, NC, 1998.
- (46) Ammeter, J.; Bürgi, H.-B.; Thibeault, J.; Hoffmann, R. *J. Am. Chem. Soc.* **1978**, *100*, 3686–3692.